Ain Shams Engineering Journal 16 (2025) 103235

Contents lists available at ScienceDirect

Ain Shams Engineering Journal

journal homepage: www.sciencedirect.com

Full Length Article

Automated hip dysplasia detection using novel FlexiLBPHOG model with ultrasound images

Sefa Key [a], Huseyin Kurum [e], Omer Esmez [e], Abdul Hafeez Baig [b], Rena Hajiyeva [c], Sengul Dogan [d,*], Turker Tuncer [d]

[a] Orthopedics and Traumatology Department, Firat University Hospital, Firat University, Elazığ, Turkey
[b] School of Business, University of Southern Queensland, West Street Toowoomba, QLD, Australia
[c] Western Caspian University, Department of Information Technologies, Baku, Azerbaijan
[d] Department of Digital Forensics Engineering, Technology Faculty, Firat University, Elazig, Turkey
[e] Orthopedics and Traumatology Department, Elazig Fethi Sekin City Hospital, 23100 Elazig, Turkey

ARTICLE INFO

Keywords:
Development hip dysplasia detection
FlexiLBPHOG
Multiple feature selection
Information fusion
Ultrasound

ABSTRACT

This study focuses on automatically detecting developmental hip dysplasia (DHD) using a novel feature engineering model, FlexiLBPHOG, inspired by the FlexiViT model. The model utilizes five patch types for feature extraction with local binary pattern (LBP) and histogram of oriented gradients (HOG) techniques. During feature extraction, five feature vectors are generated. In the next stage, three feature selection methods—Neighborhood Component Analysis (NCA), Chi-square (Chi2), and ReliefF (RF)—are used to select the top 500 features. Classification is performed using support vector machine (SVM) and k-nearest neighbors (kNN), resulting in 30 outcomes. Information fusion through iterative majority voting (IMV) and a greedy algorithm yields 58 outcomes, from which the best is selected. The FlexiLBPHOG model achieved a classification accuracy of 94.38% in detecting DHD in ultrasound images from a private dataset. The study confirms the effectiveness of the proposed model in image classification by integrating shallow image descriptors.

1. Introduction

Developmental hip dysplasia (DDH) is affecting 1–3 % of infants [1,2]. Misdiagnosis or failure to diagnose DDH is thought to account for more than one-third of hip replacement operations performed under the age of 60 [3]. If diagnosed early, DDH can be treated with simple methods (Pavlik bandage). In the neonatal period, the chance of cure is very high (>90 %) in infants younger than *seven* weeks but decreases thereafter [4,5]. Despite the obvious advantages of early diagnosis, high variability in partial assessment has been reported [6]. Ultrasound is non-invasive, portable, and sensitive to DDH, making it ideal for hip screening in diagnosing and managing DDH in infants. Currently, two-dimensional ultrasound (2DUS) is used to diagnose DDH. Scans are performed according to the Graf criteria, based on measuring the angle between the ilium and the acetabular roof (called the alpha angle), as shown in Fig. 1. Alpha angles $> 60^\circ$ are considered normal [7]. Ultrasound is valuable in the first few months of life. When the ossified nucleus of the femoral head appears, the value of ultrasound decreases, and radiography is recommended [8,9]. Conventional 2D ultrasound involves static image assessment according to Graf's criteria, primarily based on measuring the angle between the ilium and the acetabular roof (alpha angle; see Fig. 1). Alpha angles $> 60^\circ$ are considered normal, while angles $< 43^\circ$ indicate severe dysplasia. The visualization should include the ilium, acetabular roof, labrum, and femoral head, which are challenging to assess. Although this depends on the examiner, there is a risk of misdiagnosis in two-thirds of neonates and half of infants [10]. Considering the importance of early diagnosis of DDH and that negative results may occur with possible misdiagnosis, we conducted our study with this hypothesis. It has been shown that the α-angle shows a monthly increase and the β-angle a monthly decrease in the first *three* months of life [11]. With this in mind, our study analyzed hip ultrasound images of children aged 3–6 months. The aim was to present a method for differentiating between normal and abnormal hips in hip ultrasound images automatically without human errors.

* Corresponding author.
E-mail addresses: skey@firat.edu.tr (S. Key), dr.hsynkrm@gmail.com (H. Kurum), oesmez@firat.edu.tr (O. Esmez), Abdul.Hafeez-Baig@usq.edu.au (A.H. Baig), rena.haciyeva@wcu.edu.az (R. Hajiyeva), sdogan@firat.edu.tr (S. Dogan), turkertuncer@firat.edu.tr (T. Tuncer).

https://doi.org/10.1016/j.asej.2024.103235
Received 5 September 2024; Received in revised form 7 November 2024; Accepted 10 December 2024
Available online 19 December 2024
2090-4479/© 2024 The Authors. Published by Elsevier B.V. on behalf of Faculty of Engineering, Ain Shams University. This is an open access article under the CC BY-NC-ND license (http://creativecommons.org/licenses/by-nc-nd/4.0/).

1.1. Literature review

Many different models [12–15,44] and machine learning techniques [16–18,45] are suggested for disciplines in the literature. Hareendranathan et al. [19] conducted a deep-learning (DL) method to diagnose DDH using 2D ultrasound images. They applied this method using 50 infant hips and achieved promising results in accurately segmenting the acetabulum bone and classifying hips as normal or dysplastic. Their study highlighted the potential of automated systems to improve the consistency and accuracy of DDH diagnosis in clinical settings. Sezer and Sezer [20] achieved a notable breakthrough in the automatic classification of neonatal hip ultrasound images. Their study, which utilized deep convolutional neural networks, reported a remarkable accuracy of 96.6 % in distinguishing between normal and dysplastic hips. Their significant achievement was made possible by their innovative data augmentation method, incorporating speckle noise reduction, which enhanced the CNN's performance in diagnosing DDH. Their advancement marked a substantial contribution to medical image analysis using DL techniques. Atalar et al. [21] focused on using DL for diagnosing DDH from ultrasound images. Their research involved DL models developed usingthe dataset of 376 normal, 541 dysplasia, and 365 incorrect probe position ultrasound images. The VGG-19 model notably achieved 93 % accuracy, 93.5 % sensitivity, 96.7 % specificity, 92.3 % precision, 92.6 % F1 score, and 0.99 AUC, demonstrating the effectiveness of DL in diagnosing DDH from ultrasound images. Lee et al. [22] evaluated a DL-based system for DDH screening using ultrasound images. Their system was tested on 921 ultrasound images, leading to the classification of 320 images as suitable for screening by both artificial intelligence (AI) and a human observer. Their study found excellent agreement (the intraclass correlation coefficient = 0.764) for alpha angle and good agreement (ICC = 0.743) for beta angle measurements between the AI system and a human observer. These results indicate the AI system's high reliability and potential to aid in DDH screening. Xu et al. [23] developed a novel method for detecting hip landmarks in ultrasound images, utilizing a Dependency Mining ResNet (DM-ResNet) model. Their method was tested on a dataset of 2000 annotated hip ultrasound images, achieving an average point error of 0.719 mm and a successful detection rate of 79.9 % within a 1 mm threshold. These results highlighted the potential of DM-ResNet in improving the accuracy of DDH diagnosis. Park et al. [24] evaluated a DL algorithm's diagnostic performance on 5076 hip anteroposterior radiographs for detecting DDH. The results showed that the algorithm obtained a sensitivity of 98.0 %, specificity of 98.1 %, positive predictive value (PPV) of 84.5 %, and negative predictive value (NPV) of 99.8 %. The area under the ROC plot was 0.988, demonstrating the algorithm's high reliability and accuracy in DDH detection. El-Hariri [25] focused on enhancing the diagnosis of DDH using 3D ultrasound and DL. He implemented advanced 3D convolutional neural networks for segmentation, metric extraction, and adequacy classification in ultrasound imaging. Their approach significantly improved the accuracy and reliability of hip dysplasia measurements, demonstrating a notable advancement over traditional methods in DDH diagnosis. The thesis provided detailed metrics and statistical data to support these findings. Bilynsky et al. [26] focused on evaluating the effectiveness of convolutional neural networks like GoogleNet, SqueezeNet, and AlexNet in classifying and recognizing ultrasound images of the hip joint. Their study used a dataset of 97 standard ultrasonic images. The convolutional neural network, GoogleNet showed remarkable results, achieving up to 100 % accuracy in the training group and 84.5 % accuracy in the test group, indicating the potential of CNNs in aiding the computer-aided diagnosis of pediatric dysplasia. Hareendranathan et al. [10] involved training convolutional neural network models to detect the presence of four key

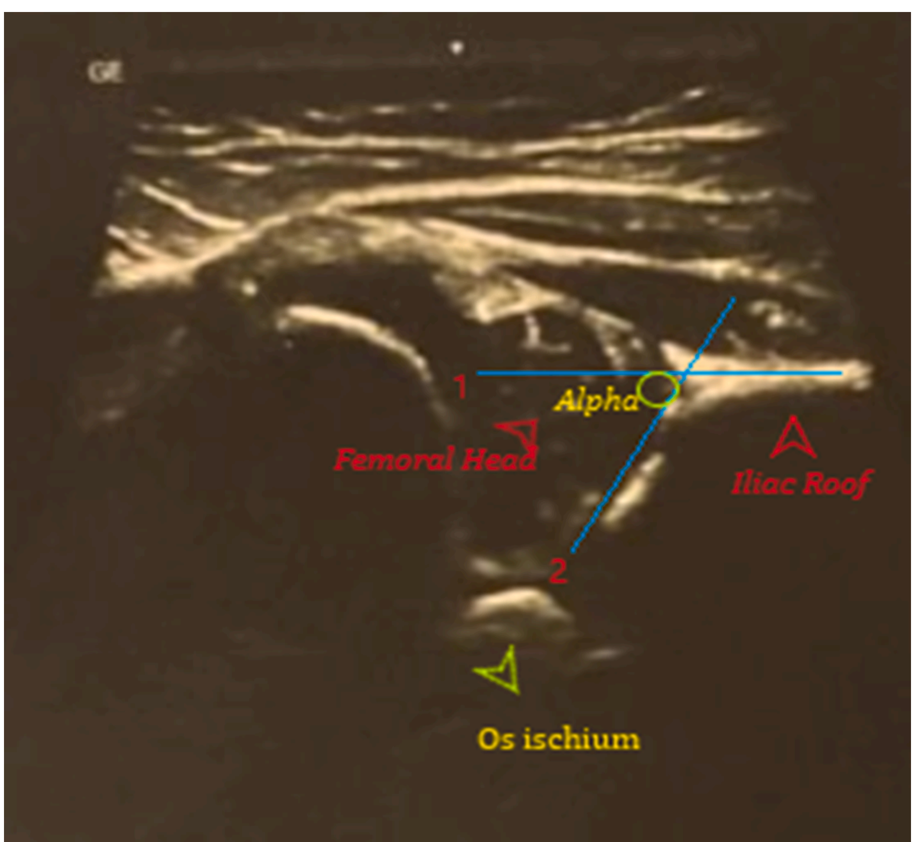

Fig. 1. Ultrasound image of the hip in the coronal Graf plane with anatomical landmarks such as the iliac roof, labrum, acetabulum, femoral head, and ischial tuberosity. The alpha angle is measured as the angle between the iliac roof and the acetabulum (Lines 1 and 2).

ultrasound landmarks in hip images. Their study utilized 100 3D ultrasound images for training and validated the technique on 107 images. Their results demonstrated that the AI achieved over 85 % accuracy for all landmarks and showed substantial agreement with manual assessments, indicating the potential of AI in improving ultrasound scan quality assessment for DDH screening. Jaremko et al. [27] focused on using machine learning algorithms to analyze ultrasound images for hip dysplasia screening. Their study involved processing a significant number of ultrasound images and comparing the algorithm's performance against traditional diagnostic methods. Their results demonstrated improved diagnostic accuracy, indicating the potential of machine learning in enhancing the effectiveness of sonographic screening for hip dysplasia. Hu et al. [28] employed a multi-task learning network to enhance the automatic evaluation of DDH from ultrasound images. Their work involved a sample of 1231 US images from 632 patients. Their method demonstrated significant accuracy, with the average errors in alpha and beta angles being 2.221° and 2.899° respectively. Approximately 93 % of alpha angle estimates and 85 % of beta angle estimates had errors less than 5 degrees, showing the potential of this method for clinical application in DDH diagnosis.

1.2. Literature gaps

Our literature review revealed several shortcomings in detecting developmental hip dysplasia (DHD). The identified gaps in the existing literature include:

- There is a scarcity of automated models designed explicitly for DHD detection.
- Researchers focus predominantly on using deep learning for biomedical image classification [46,47].
- A lack of diversity in feature engineering models, particularly those that utilize patch-based approaches, as most feature engineering models have distinct structures.

1.3. Motivation and our model

In this study, our primary inspiration is drawn from the FlexiViT method. The FlexiViT model employed a diverse set of fixed-size patches. We aim to introduce a novel feature engineering model based on multiple patches. To increase the impact of this study, we curated a new dataset of ultrasound (US) images for hip dysplasia detection. Additionally, we proposed a new self-organized feature engineering model, termed FlexiLBPHOG.

The FlexiLBPHOG model comprises four main phases:

- Feature extraction utilizing LBP [29] and HOG [30] image descriptors with five types of fixed-size patches.
- Feature selection based on NCA [31], Chi2 [32], and RF [33] methods.
- Classification employing kNN [34] and SVM [35].
- Information fusion using IMV [36] and a greedy algorithm [37].

By implementing these phases, we have developed the FlexiLBPHOG model and applied it to the acquired US image dataset.

1.4. Novelties and contributions

This work introduces two pivotal innovations: (i) the newly proposed FlexiLBPHOG and (ii) the collected US image dataset for DHD detection. This study represents a pioneering effort in Flexi-based feature engineering and DHD research.

The novelty and main contribution of this work are as follows:

Novelties:

- A novel DHD US image dataset was developed.
- A new feature engineering model, FlexiLBPHOG, has been introduced for DHD, serving as the feature engineering version of FlexiViT.

Contributions:

- DHD is a prevalent disorder worldwide. The early and accurate detection is crucial to improve patient care. A novel machine-learning approach has been proposed to detect DHD automatically to address this problem.
- The introduction of FlexiLBPHOG aims to enhance the classification ability of the feature engineering model. It demonstrated outstanding performance, achieving a classification accuracy of 94.38 %. For this dataset, the introduced FlexiLBPHOG has compared to deep learning models and it yielded superior classification performance.

2. Dataset

We collected this dataset from children admitted to the hospital between 01/01/2020 and 01/01/2023. This dataset contained two classes: (i) DHD and (ii) non-DHD. Three orthopedists labeled these two classes of US images. The dataset consists of 801 US hip images (172 DHD images and 629 non-DHD) of children aged 3–6 months (average age was 4.5 months). These images were collected from 801 participants. Typical sampled images are shown in Fig. 2.

3. FlexiLBPHOG

We have introduced an innovative self-organized feature engineering model comprising four sequential phases. In the first phase, known as Flexi-Based Feature Extraction, we employed five types of patches (14×14, 16×16, 28×28, 32×32, and 56×56) extracted from 224×224-sized images. This process yielded diverse fixed-size patches (256, 196, 64, 49, and 16). We extracted textural and directional features from each patch using LBP and HOG feature extractors, creating five feature vectors. The FlexiLBPHOG model extracts both fine-grained and coarse-grained features from images using various patch sizes. Smaller patches (e.g., 14×14 and 16×16) focus on local details, capturing both textural and directional nuances that can help identify DHD indicators that may not be visible to the naked eye. Larger patches (e.g., 28×28, 32×32, and 56×56) capture broader structural information, allowing the model to account for larger anatomical patterns and directional gradients within the image.

The feature selection process was performed using three feature selectors commonly used in the literature: NCA, Chi2, and RF. The main purpose of using these selectors was to create a richer set of selected features. In this study, various feature set sizes were tested to determine the optimal number of features that maximize classification performance. After testing, it was found that selecting the top 500 features yielded the best results for DHD detection. Although iterative feature selectors could have been used at this stage, their high time complexity led to the decision to select only the most significant 500 features. By applying each feature selection method to the five patch sizes, a total of 15 (5×3) feature vectors, each containing 500 features, were created.

In the third phase, classification using kNN and SVM classifiers is performed. We applied these classifiers to the 15 selected features and produced 30 classifier-specific outcomes.

The fourth and final phase, Information Fusion, involved implementing IMV on the 30 classifier-specific outcomes, generating 28 voted outcomes with an initial IMV loop value of 3. Subsequently, a greedy algorithm was employed to select the best outcome from 58 outcomes (30 classifier-specific + 28 voted).

To better explain the proposed FlexiLBPHOG model, please refer to Fig. 3, which provides a graphical overview.

* PD: patch division, p: fixed-size patch, f: feature of each patch, F:

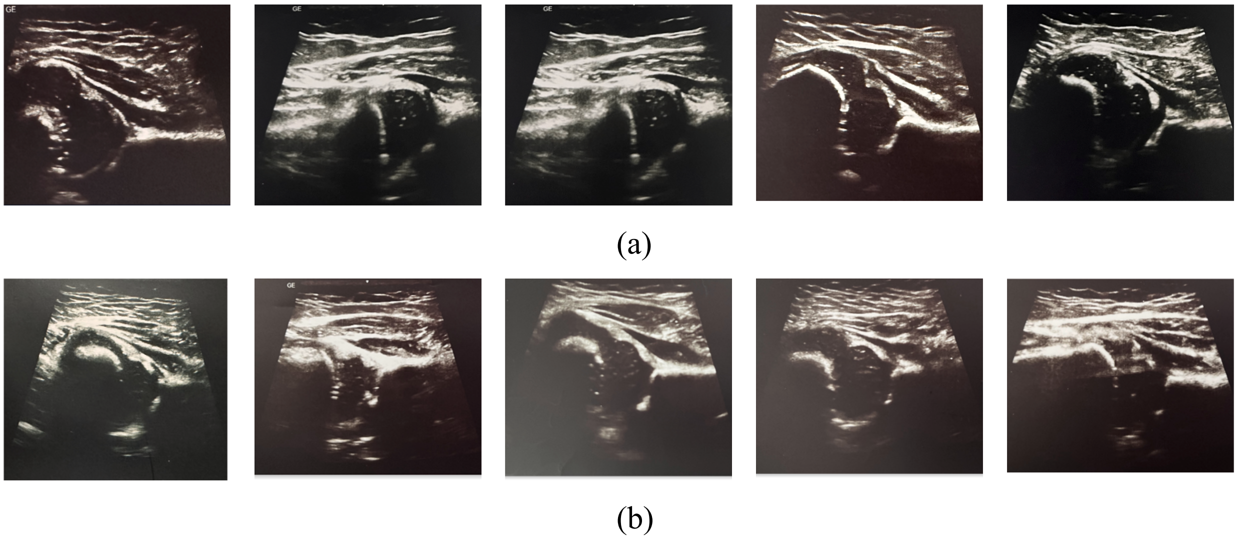

Fig. 2. Sample US images collected from the private dataset: (a) DHD, and (b) Non-DHD.

the merged feature vector, s: selected feature vector, c: classifier-wise outcome, v: voted outcome. To create f, we have applied LBP and HOG feature extractors to each patch and we have merged the extracted textural (by generating LBP) and directional (by extracting HOG) features.

More details of this work are given below.

Feature extraction: The important step in the proposed FlexiLBPHOG is its feature extraction phase. In this crucial stage, we employed LBP, HOG, and a division of fixed-size patches into five types. Through the application of these methods, we derived five distinct feature vectors. This phase's primary goals encompass extracting textural and directional features by utilizing patches of varying sizes and capturing meaningful features. The steps of this phase are elaborated below to provide a more comprehensive clarification.

Step 1: Transform each image to grayscale and resize images to 224 × 224 sized images.

Step 2: Divide the image into five types of fixed-size patches.

$$p_{n^k}^k(i,j) = Im\left(i^k + t^k - 1, j^k + t^k - 1\right), k \in \{1, 2, \cdots, 5\},$$

$$a \in \{14, 16, 28, 32, 56\}, i^k \in \{1, 2, \cdots, a(k)\}, j^k \in \{1, 2, \cdots, a(k)\},$$

$$t^k \in \{1, a(k), \cdots, 224 - a(k) + 1\}, n^k \in \{1, 2, \cdots, h(k)\},$$

$$h \in \{16, 49, 64, 196, 256\} \tag{1}$$

Herein, p: fixed-size patches. We have generated five types of patches deploying 14 × 14, 16 × 16, 28 × 28, 32 × 32, and 56 × 56 sized patches.

Step 3: Extract features deploying LBP and HOG extractors.

$$f_{n^k}^k = \omega\left(\lambda\left(p_{n^k}^k\right), \xi\left(p_{n^k}^k\right)\right) \tag{2}$$

where f: feature vector of each patch, $\lambda(.)$: HOG feature extractor, $\xi(.)$: LBP feature extractor and $\omega(.)$: concatenation function.

Step 4: Merge the generated feature vectors to create the final feature vectors.

$$F^k = \omega\left(f_1^k, f_2^k, \cdots, f_{n^k}^k\right) \tag{3}$$

Here, F: merged feature vector.

Step 5: Repeat steps 1–4 until the number of images and create feature matrices. In this phase, we have generated five feature matrices.

Feature selection: In this phase, we employed three well-known feature selectors, namely Chi2, NCA, and RF. We created five feature vectors with diverse sizes as part of the feature extraction process. We generated 15 feature vectors in this section by selecting the most informative 500 features. The steps of this phase are as follows:

Step 6: Generate the qualified indexes by deploying the Chi2, NCA, and RF feature selectors.

$$id^c = \chi(F_k, y), c \in \{1, 4, \cdots, 13\},$$

$$id^{c+1} = \eta(F_k, y),$$

$$id^{c+2} = \rho(F_k, y) \tag{4}$$

where id: the qualified indexes, $\chi(.)$: Chi2 feature selector, $\eta(.)$: NCA feature selector, $\rho(.)$: RF feature selector and y: actual/real labels.

Step 7: Select the most informative features from the generated feature vectors utilizing the generated qualified indexes.

$$S^c(d,i) = F_k(d, id^c(i)), d \in \{1, 2, \cdots, N\}, i \in \{1, 2, \cdots, 500\}$$

$$S^{c+1}(d,i) = F_k\left(d, id^{c+1}(i)\right),$$

$$S^{c+2}(d,i) = F_k\left(d, id^{c+2}(i)\right) \tag{5}$$

Herein, S: selected feature vector with a length of 500, and N: the number of images.

In this phase, 15 (=5 × 3) selected feature vectors have been created, and the length of each feature vector is 500 since we have selected the most informative 500 features.

Classification: To produce outcomes specific to each classifier, we utilized kNN and SVM classifiers. These classifiers were applied to the set of 15 selected features, creating 30 outcomes (15 for each classifier). The parameters of the employed classifiers are provided below.

kNN: k;1, distance; L1-norm, validation; ten-fold cross-validation, voting: none.

SVM: Kernel; cubic polynomial kernel; box-constraint; 1, kernel scale; automatic coding; one-vs-one; validation; ten-fold cross-validation.

The classification step of the presented FlexiLBPHOG is:

Step 8: Generate the classifier-wise outcomes.

$$c^r = kNN(S^r, y), r \in \{1, 2, \cdots, 15\},$$

$$c^{r+15} = SVM(S^r, y) \tag{6}$$

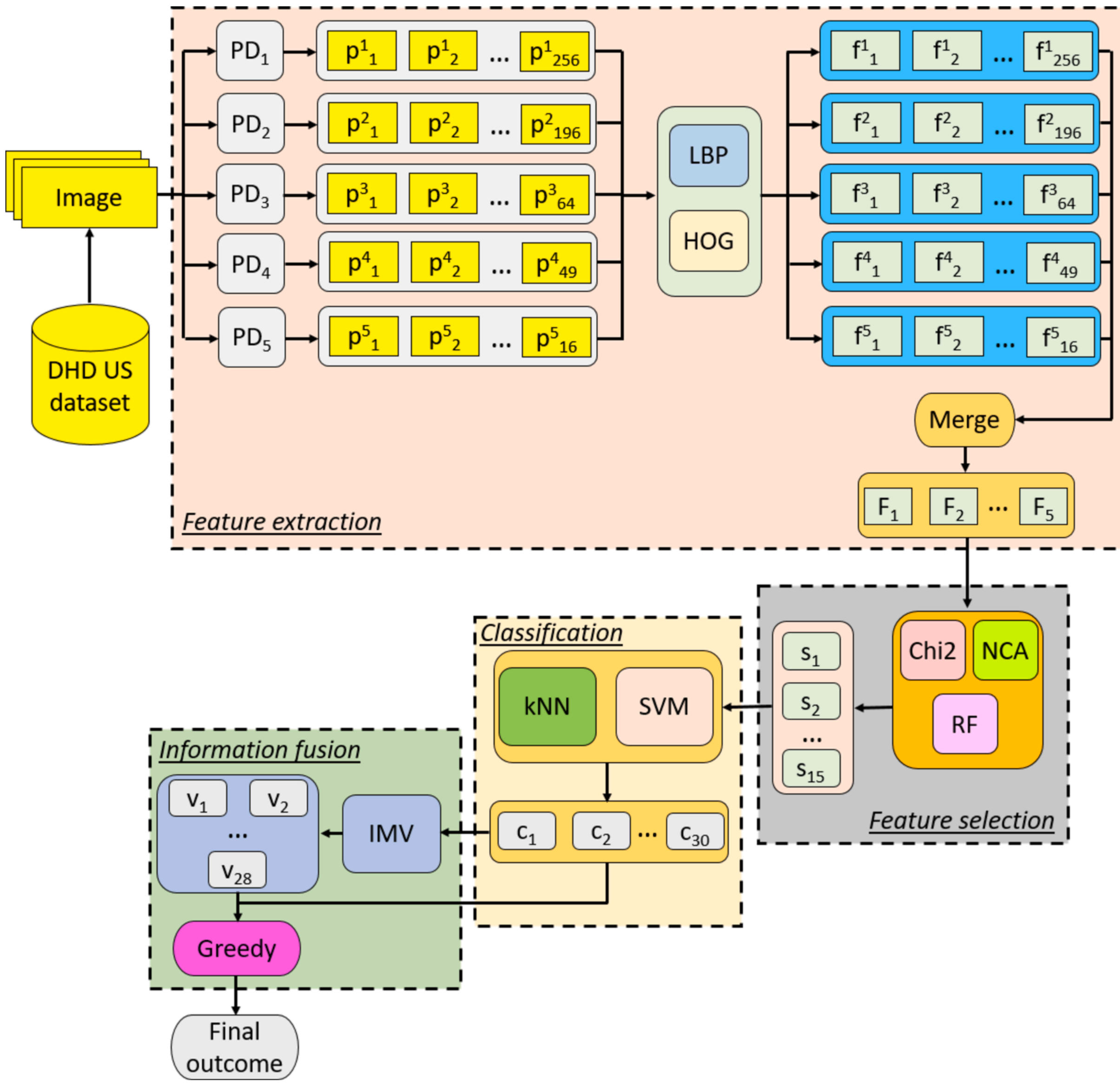

Fig. 3. Graphical overview of the proposed FlexiLBPHOG.

where c: classifier-specific outcome.

Information fusion: We have used IMV and greedy algorithm in this phase. IMV was proposed by Dogan et al. [38]. We have used the generated classifier-specific outcomes as input of the IMV algorithm and generated 28 (=30–3 + 1) voted outcomes. The steps of this phase are:

Step 8: Produce the voted outcomes.

$$v^{a-2} = \psi(c^a), a \in \{1, 2, \cdots, 30\} \tag{7}$$

Herein, v: voted outcome and $\psi(.)$: IMV majority voting function.

Step 9: Select the most accurate outcome as the final outcome by deploying a greedy algorithm.

$$acc(a) = \phi(c^a, y),$$

$$acc(t+30) = \phi(v^t, y), t \in \{1, 2, \cdots, 28\},$$

$$[mak, ind] = max(acc),$$

$$fout = \begin{cases} c^{ind}, ind \leq 30 \\ v^{ind-30}, ind > 30 \end{cases} \tag{8}$$

*acc: classification accuracy, $\phi(.)$: classification accuracy calculation function, mak: maximum accuracy, ind: index of the maximum accuracy and $fout$: final outcome.

The explained nine steps above have been defined in the proposed FlexiLBPHOG feature engineering model.

4. Experimental results

We have introduced a novel feature engineering model implemented on a standard personal computer (PC) with a configuration comprising 32 GB of main memory, a 2.1 GHz processor, and a 1-terabyte disk running the Windows 11 operating system. To implement this model, we used the MATLAB programming environment, specifically MATLAB version 2023b.

The proposed FlexiLBPHOG was implemented through m files. During the feature extraction phase, the ExtractLBPFeatures and ExtractHOGFeatures functions, integral to MATLAB, were employed to generate features. The Chi2, NCA, and RF feature selectors were employed to identify the most informative features. Additionally, the classification learner tool in MATLAB was used to select the best classifiers, and the corresponding codes were generated. An m file was created for information fusion to apply the IMV and greedy algorithm.

The dataset employed in this study consists of two classes, thereby constituting a binary classification problem. To assess the performance of the presented FlexiLBPHOG, we employed performance evaluation metrics, including accuracy, sensitivity, specificity, and geometric mean.

The presented FlexiLBPHOG yields both classifier-wise and voted outcomes. Consequently, we evaluated these outcomes using separate tables, presenting the classification performances in Table 1 and Table 2.

Table 1 demonstrates that the best classifier-specific result is the 20th result, which achieved 93.51 % classification accuracy and 87.28 % geometric mean. The results of the voted outcomes are tabulated in Table 2.

It may be noted from Table 2 that, the highest voting accuracy of 94.38 % is achieved. The application of IMV led to an improvement in the top classification accuracy from 93.51 % to 94.38 %, and there was an increase in the best sensitivity from 77.91 % to 81.98 %. As indicated by these tables (refer to Table 1 and Table 2), the most accurate classification results are associated with a voted outcome. The corresponding confusion matrix for this outcome is presented in Fig. 4.

*1: DHD, 2: Non-DHD.

The results of the final outcome are as follows: Accuracy: 94.38 %, Sensitivity: 81.98 %, Specificity: 97.77 %, and Geometric Mean: 89.53 %. Additionally, we computed the precision and F1-score for this outcome, which are as follows: Precision: 92.90 % and F1-score: 87.10 %.

The second evaluation metric is time complexity, and we utilized Big O notation to assess the computational complexity for the FlexiLBPHOG model. The analysis of the time complexity for this model is presented below.

Feature extraction: In the feature extraction phase, we divided fixed-size patches into five types, including LBP and HOG methods. The time complexity of both LBP and HOG methods is denoted as $O(H)$, where H represents the size of the image. Additionally, features were extracted from the patches. Consequently, the calculated time complexity is $O(2kNH)$, where k is the number of patch types, and N is the number of patches.

Feature selection: In this phase, we utilized three distinct feature selection functions, each with its unique structure. To represent the feature selection complexity, we introduced C as a variable. The time complexity of this phase is expressed as $O(3FC)$, where F denotes the number of feature vectors.

Classification: In the classification phase, we employed two classifiers, and the variable S was introduced to denote the time complexity of this model. The computed complexity of the classification phase is represented as $O(2FS)$.

Iterative majority voting: The least complex and last phase of the proposed FlexiLBPHOG is the information fusion, where we utilized IMV and a greedy algorithm. The time complexity of this phase is expressed as $O(IL + L)$, where I represents the number of iterations and L denotes the number of outcomes.

Overall, the time complexity of this model is $O(2kNH + 3FC + 2FS + IL + L) \cong O(kNH + FC + FS + IL)$. This result indicates that our proposed FlexiLBPHOG exhibits linear complexity.

5. Discussions

In this work, we introduced a novel self-organized feature engineering FlexiLBPHOG model. Our model produced 58 outcomes, with 30 being classifier-specific and 28 representing voted outcomes. Machine learning methods were employed in this process. In this section, we discussed the performance analysis of all the methods employed and presented in Table 3.

As shown in Table 3, we used kNN and SVM classifiers in this model. To select these classifiers, we tested several shallow classifiers, which included: 1) Decision Tree (DT), 2) Logistic Regression (LR), 3) Multilayer Perceptron (MLP), 4) Naïve Bayes (NB), 5) Linear Discriminant Analysis (LDA), 6) Bagged Tree (BT), 7) kNN, and 8) SVM. The classification performance of these classifiers was evaluated using the fifth selected feature vector. The classification accuracies of these classifiers are shown in Fig. 5.

According to Fig. 5, the two best classifiers are kNN and SVM. Therefore, we used these classifiers to generate classifier-based outcomes. No hyperparameter optimization or fine-tuning methods were applied; default parameters were used.

The summary of various combinations of patch sizes, feature selection, and classifiers is shown in Table 3. The box plot of classification accuracy (%) obtained using various: (a) patches, (b) feature selection methods, and (c) classifiers are shown in Fig. 6.

Based on the analyses, the highest classification accuracy was achieved using16 × 16-sized patches, while the greatest average accuracy was obtained with 28 × 28-sized patches. In terms of feature selection, NCA outperformed other feature selectors. Among the classifiers, the SVM demonstrated superiority over the kNN classifier.

The second-voted outcome represents the ultimate result of the presented model (FlexiLBPHOG). This second-voted outcome was derived from the top four classifier-wise outcomes, each generated using the following methods:

- *Outcome 20:* 16 × 16-sized patch, NCA selector, SVM,
- *Outcome 17:* 14 × 14-sized patch, NCA selector, SVM,
- *Outcome 23:* 28 × 28-sized patch, NCA selector, SVM,
- *Outcome 19:* 16 × 16-sized patch, Chi2 selector, SVM.

Table 1
Classifier-specific results (%) obtained for the proposed FlexiLBPHOG model.

No	Acc.	Sen.	Spec.	GM	No	Acc.	Sen.	Spec.	GM
1	88.39	64.53	94.91	78.26	**16**	90.14	68.02	96.18	80.89
2	89.89	59.88	98.09	76.64	**17**	92.38	73.26	97.62	84.56
3	87.52	44.77	**99.21**	66.64	**18**	88.26	55.81	97.14	73.63
4	88.76	69.77	93.96	80.96	**19**	91.76	74.42	96.50	84.74
5	90.01	63.95	97.14	78.82	**20**	**93.51**	**77.91**	97.77	**87.28**
6	84.89	40.12	97.14	62.42	**21**	88.01	55.81	96.82	73.51
7	88.89	72.67	93.32	82.35	**22**	91.14	73.84	95.87	84.13
8	88.39	50.58	98.73	70.67	**23**	92.38	71.51	98.09	83.75
9	89.64	62.21	97.14	77.74	**24**	89.01	61.05	96.66	76.82
10	88.26	64.53	94.75	78.20	**25**	90.14	69.77	95.71	81.71
11	88.01	52.33	97.77	71.53	**26**	91.51	68.02	97.93	81.62
12	89.14	60.47	96.98	76.58	**27**	90.39	64.53	97.46	79.31
13	88.64	65.12	95.07	78.68	**28**	89.01	64.53	95.71	78.59
14	88.76	55.81	97.77	73.87	**29**	91.26	68.02	97.62	81.49
15	87.64	56.98	96.03	73.97	**30**	89.89	65.12	96.66	79.34

** Acc.: Accuracy, Sen.: Sensitivity, Spe.: Specificity, GM: geometric mean. The best results are highlighted using bold font color.

Table 2
Voted results (%) obtained for the developed FlexiLBPHOG model.

No	Acc.	Sen.	Spec.	GM	No	Acc.	Sen.	Spec.	GM
1	93.63	76.74	98.25	86.83	**15**	92.88	70.93	98.89	83.75
2	**94.38**	**81.98**	97.77	**89.53**	**16**	93.38	73.84	98.73	85.38
3	94.38	79.07	98.57	88.28	**17**	92.76	70.93	98.73	83.68
4	94.13	79.65	98.09	88.39	**18**	93.01	72.09	98.73	84.37
5	93.76	76.16	98.57	86.64	**19**	92.76	69.77	99.05	83.13
6	93.88	78.49	98.09	87.74	**20**	93.38	72.67	99.05	84.84
7	93.51	75	98.57	85.98	**21**	92.26	67.44	99.05	81.73
8	93.51	76.74	98.09	86.76	**22**	92.63	69.19	99.05	82.78
9	93.13	74.42	98.25	85.51	**23**	92.13	66.86	99.05	81.38
10	93.26	75.58	98.09	86.10	**24**	92.26	67.44	99.05	81.73
11	93.38	73.26	98.89	85.11	**25**	91.76	65.12	99.05	80.31
12	93.88	76.16	98.73	86.71	**26**	92.13	67.44	98.89	81.66
13	93.26	72.67	98.89	84.77	**27**	91.14	61.63	**99.21**	78.19
14	93.76	75.58	98.73	86.38	**28**	91.14	62.21	99.05	78.50

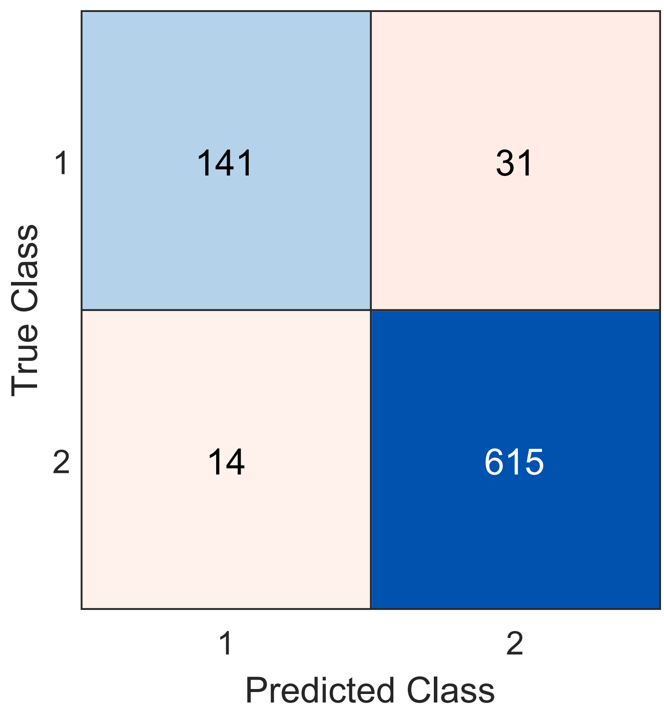

Fig. 4. Confusion matrix of the outcome.

– In our analysis, the optimal outcome was achieved with 16 × 16-sized patches, NCA as the selector, and SVM classifier. Our analysis indicates that it is not needed to employ (i) 56 × 56-sized patches, (ii) RF selector, and (iii) kNN classifier to obtain the final outcome.
– Chi2 evaluates features based on their independence from others, while RF considers feature importance scores. NCA, a distance-based feature selector, optimizes feature selection by considering label

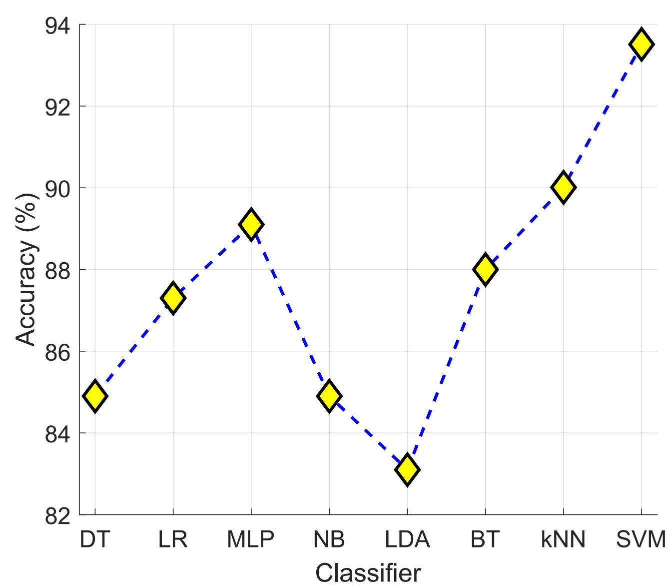

Fig. 5. The classification accuracies of the classifiers on the used DHD dataset.

Table 3
Summary of various combinations of patch sizes, features selection and classifiers.

No	Patch size	Feature selection	Classifier	No	Feature extraction	Feature selection	Classifier
1	14 × 14	Chi2	kNN	**16**	14 × 14	Chi2	SVM
2	14 × 14	NCA	kNN	**17**	14 × 14	NCA	SVM
3	14 × 14	RF	kNN	**18**	14 × 14	RF	SVM
4	16 × 16	Chi2	kNN	**19**	16 × 16	Chi2	SVM
5	16 × 16	NCA	kNN	**20**	16 × 16	NCA	SVM
6	16 × 16	RF	kNN	**21**	16 × 16	RF	SVM
7	28 × 28	Chi2	kNN	**22**	28 × 28	Chi2	SVM
8	28 × 28	NCA	kNN	**23**	28 × 28	NCA	SVM
9	28 × 28	RF	kNN	**24**	28 × 28	RF	SVM
10	32 × 32	Chi2	kNN	**25**	32 × 32	Chi2	SVM
11	32 × 32	NCA	kNN	**26**	32 × 32	NCA	SVM
12	32 × 32	RF	kNN	**27**	32 × 32	RF	SVM
13	56 × 56	Chi2	kNN	**28**	56 × 56	Chi2	SVM
14	56 × 56	NCA	kNN	29	56 × 56	NCA	SVM
15	56 × 56	RF	kNN	30	56 × 56	RF	SVM

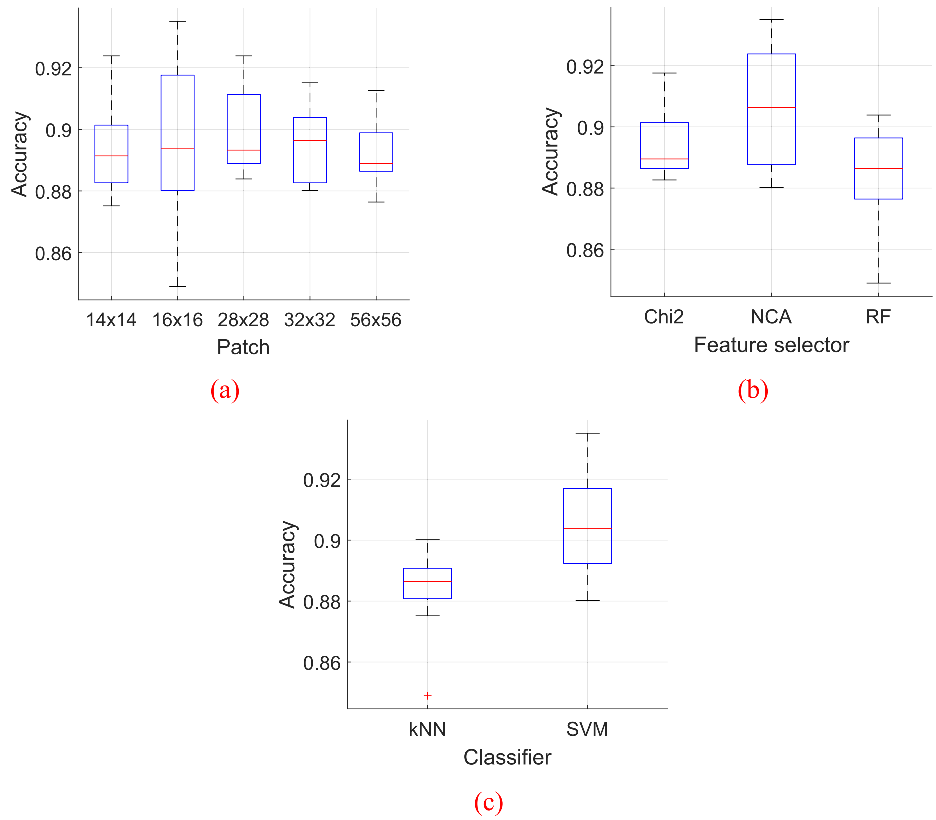

Fig. 6. Box plots of classification accuracy obtained using various: (a) patches, (b) feature selection methods, and (c) classifiers.

proximity, allowing NCA to perform more effectively. In terms of computational complexity, NCA is generally more demanding than Chi2 and RF due to its iterative optimization of feature weights to maximize classification performance. Chi2, as a statistical method, typically involves fewer computational steps, although RF's computational complexity is not low. Using NCA alongside Chi2 and RF enriches the selected feature set by blending supervised and statistical feature selection techniques.

We employed both LBP and HOG feature extractors to highlight the superiority of the suggested FlexiLBPHOG. The classification accuracies obtained using LBP, – HOG, and our proposed model are illustrated in Fig. 7.

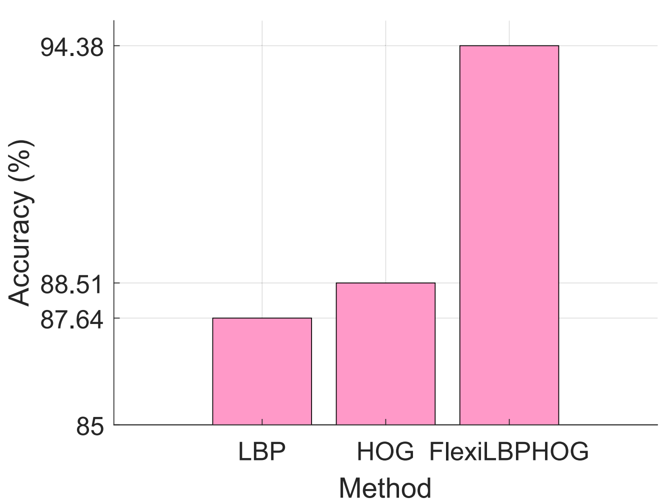

Fig. 7. Ablation results.

It may be noted from Fig. 7 that, the proposed FlexiLBPHOG increased the classification capabilities of both LBP and HOG-based models. The classification accuracy obtained with FlexiLBPHOG is significantly higher than that achieved with LBP or HOG alone. Specifically, while LBP and HOG provide accuracies below 90 %, FlexiLBPHOG achieves a substantial improvement, reaching the highest accuracy of 94.38 %. This result highlights that the combination of LBP and HOG within the FlexiLBPHOG model enhances overall classification performance and confirms the superiority of this integrated approach for the task.

The graphical representation of accuracies (%) obtained for various deep learning models deep learning [21] is shown in Fig. 8.

The deep learning models, namely VGG [39], ResNet101 [40], MobileNetV2 [41], and GoogleNet [42], achieved classification accuracies of 93 %, 89.3 %, 82.3 %, and 82.3 %, respectively. In contrast, our model achieved a higher classification performance of 94.38 % using FlexiLBPHOG. Hence, our proposed model demonstrated superior classification performance compared to these deep learning models.

Moreover, we have compared the presented FlexiLBPHOG with the Gong et al. [43] model and the comparative results are listed in Table 4.

Gong et al. [43] proposed a method incorporating hand-crafted features with a deep neural network-based ensemble model and achieved an accuracy of 85.89 %. In contrast, our model, FlexiLBPHOG, outperforms this approach with a higher accuracy of 94.38 %. It can be noted from Table 4 that, we have used more images than Gong et al. [43] and also employed ten-fold cross-validation. Hence, our model is accurate and more robust. The combination of LBP and HOG helps to extract the subtle features from the US images and obtain high classification performance.

The advantages of this work are summarized below:

- The FlexiLBPHOG model aims to increase classification performance for DHD detection in US images. The major goal of this method is to

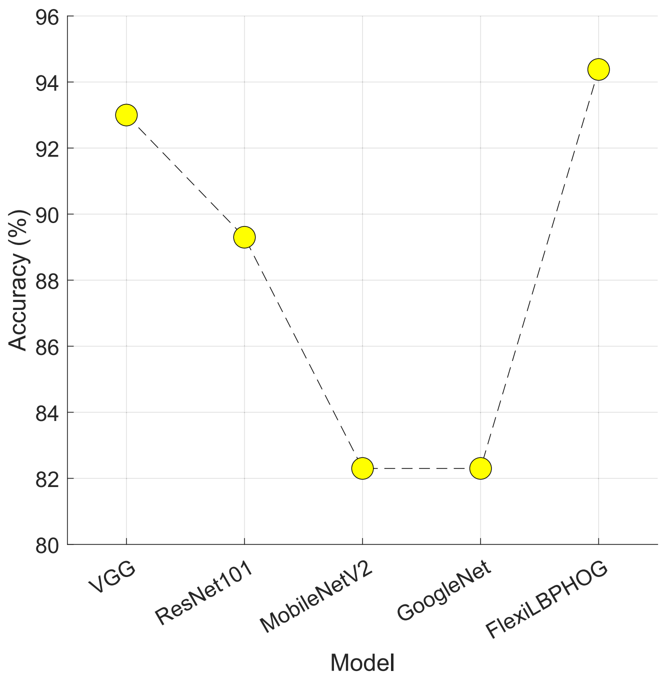

Fig. 8. Graphical representation of accuracies (%) obtained for various deep learning models.

achieve high accuracy comparable to deep learning models. The presented FlexiLBPHOG attained superior classification performance compared to deep learning models, and our proposal has linear time complexity.

- Unlike standard LBP and HOG, FlexiLBPHOG uses multiple fixed-size patches (14×14, 16×16, 28×28, 32×32, and 56×56). This patch-based approach enables the model to extract localized textural and directional features from different regions of the image, capturing all relevant features associated with DHD in ultrasound images.
- Five patch-based feature vectors are created by combining the textural and directional features extracted by the model. In the feature selection phase, the best 500 features of the feature vectors generated from each patch type are selected to balance the number of features; however, this process is not done using a single feature selector. In this phase, a three-way feature selection process is applied using NCA, Chi2, and RF to obtain a richer set of selected feature vectors.
- Classification results are obtained using SVM and kNN classifiers. Voted outcomes are obtained using IMV. The primary advantage of obtaining voted outcomes is the calculation of combined results with higher classification performance.
- FlexiLBPHOG is presented as a flexible framework that allows users to customize patch sizes, feature extractors, feature selectors, classifiers, and voting methods to adapt it to their specific data. This framework is introduced in this article. To more clearly demonstrate the classification capability of the presented framework, a model rivaling deep learning is created using two traditional image descriptors, namely LBP and HOG.
- The presented FlexiLBPHOG is a highly accurate model, achieving 94.38 % classification accuracy on the collected DHD UD image dataset.
- By deploying IMV and a greedy algorithm, the presented model is transformed into a self-organized feature engineering model.
- Demonstrated linear time complexity ($O(kNH + FC + FS + IL)$), emphasizing computational efficiency and practical feasibility for real-world applications.
- Employed a range of performance evaluation metrics, including accuracy, sensitivity, specificity, and geometric mean, to thoroughly assess the model's performance.
- The presented FlexiLBPHOG model has shown superior classification performance compared to various deep learning models and also outperforms Gong et al.'s [43] method, which combines hand-crafted features with an ensemble deep neural network and achieves an accuracy of 85.89 %, with FlexiLBPHOG achieving higher accuracy. Additionally, it has significantly enhanced the classification capacity of the LBP and HOG methods it incorporates.

The limitations of this study are as follows. The dataset is relatively small and was collected from a single medical center. In the future, we plan to collect data from multiple medical centers, and for data flow purposes, the images will be evaluated using the widely used and standardized Graf method of hip ultrasound imaging. The Graf method, based on ultrasound imaging of the hip in the coronal plane, uses anatomical landmarks such as the iliac roof, labrum, acetabulum, femoral head, and ischial tuberosity, with the alpha angle measured as the angle between the iliac roof and the acetabulum. To standardize and reduce individual measurement errors, three consecutive ultrasound images will be obtained, and ultrasound images of pediatric hips commonly performed across different centers today will be used for multicenter study purposes. Different researchers from these centers can also be included in the study for this purpose. This will not only increase the overall dataset size but also allow for greater variability in patient demographics, contributing to a more comprehensive understanding of DHD. To address the lack of diversity, particularly in terms of race and ethnicity, efforts should be made to include ultrasound images of individuals from different racial groups. This will increase the robustness of the model and its applicability across various demographic groups.

6. Conclusions

In this study, a new self-organized feature engineering model has

Table 4
Summary of comparison of our work with other work developed for automated detection of hip dysplasia using US images.

Authors	Method	Number of patients	Number of images	Validation	Results (%)
Gong et al. [43]	Hand-crafted features + deep neural network-based ensemble model	379 subjects with DHD and 379 with control	758	5-fold cross-validation	Acc.: 85.89
Our model	FlexiLBPHOG	172 subjects with DHD and 629 with control	801	10-fold cross-validation	Acc.: 94.38, Sen.: 81.98, Spe.: 97.77, GM: 89.53, Pre.: 92.90, F1: 87.10.

** Acc.: Accuracy, Sen. Sensitivity, GM: Geometric Mean, Pre.: Precision, F1: F1-score.

been presented, and the presented model has been termed FlexiLBPHOG. The recommended FlexiLBPHOG is the feature engineering version of FlexiViT. To increase the visibility of the recommended FlexiLBPHOG, a new US image dataset was collected to detect DHD. In this respect, this model is one of the pioneering studies for early DHD detection. The recommended FlexiLBPHOG model has been shown to outperform other approaches, achieving a 94.38 % classification accuracy on the collected dataset. Specifically, the best individual classification result was obtained using a 16 × 16 patch size, NCA feature selector, and an SVM classifier. Although the 28 × 28 patch size provides the best average classification accuracy, the most accurate results were obtained with the 16 × 16 patch size, demonstrating the model's flexibility and adaptability with different patch sizes.

The self-organized feature of FlexiLBPHOG is exhibited by its selection of the most accurate result from 58 generated results, utilizing a greedy algorithm for IMV and information fusion. The combination of LBP and HOG feature extraction in FlexiLBPHOG increases robustness in detecting subtle indicators of DHD by enabling the extraction of both textural and directional information from US images.

The advantages of the FlexiLBPHOG model include high classification performance, efficient feature selection, low computational demand, and a self-organized structure. Additionally, various methods have been integrated within the framework of FlexiLBPHOG, paving the way for the development of other Flexi-based feature engineering models.

Superior accuracy in DHD detection is not only achieved by FlexiLBPHOG, but a scalable, high-performance, and computationally efficient feature engineering model for automatic ultrasound image classification is also provided. Furthermore, the potential of feature engineering is highlighted by this model, which serves as a source of inspiration for the next generation of feature engineering models to be developed in the future.

7. Dataset

We collected this dataset from Firat University Hospital from children admitted to the hospital between 01/01/2020 and 01/01/2023.

8. Institutional Review Board Statement

Institutional Review Board Statement: The study was approved by the local ethical committee, Ethics Committee of Firat University (2023/12–31).

CRediT authorship contribution statement

Sefa Key: Writing – review & editing, Writing – original draft, Visualization, Validation, Resources, Methodology, Investigation, Formal analysis, Data curation, Conceptualization. **Huseyin Kurum:** Writing – review & editing, Writing – original draft, Visualization, Validation, Resources, Methodology, Investigation, Formal analysis, Data curation, Conceptualization. **Omer Esmez:** Writing – review & editing, Writing – original draft, Visualization, Validation, Resources, Methodology, Investigation, Formal analysis, Data curation, Conceptualization. **Abdul Hafeez Baig:** Writing – review & editing, Writing – original draft, Visualization, Validation, Resources, Methodology, Investigation, Formal analysis, Data curation, Conceptualization. **Rena Hajiyeva:** Writing – review & editing, Writing – original draft, Visualization, Validation, Resources, Methodology, Investigation, Conceptualization. **Sengul Dogan:** Writing – review & editing, Writing – original draft, Visualization, Validation, Software, Resources, Methodology, Investigation, Conceptualization. **Turker Tuncer:** Writing – review & editing, Writing – original draft, Visualization, Validation, Supervision, Software, Resources, Project administration, Methodology, Investigation, Data curation, Conceptualization.

Funding

This study was supported by the Scientific Research Projects Coordination Unit of Firat University. Project number TEKF.24.49.

Declaration of competing interest

The authors declare that they have no known competing financial interests or personal relationships that could have appeared to influence the work reported in this paper.

References

[1] Furnes O, Lie S, Espehaug B, Vollset S, Engesaeter L, Havelin L. Hip disease and the prognosis of total hip replacements: a review of 53 698 primary total hip replacements reported to the Norwegian arthroplasty register 1987–99. J Bone Joint Surg 2001;83:579-..
[2] Graham SM, Manara J, Chokotho L, Harrison WJ. Back-carrying infants to prevent developmental hip dysplasia and its sequelae: is a new public health initiative needed? J Pediatr Orthop 2015;35:57–61.
[3] Price CT, Ramo BA. Prevention of hip dysplasia in children and adults. Orthopedic Clinics 2012;43:269–79.
[4] Atalar H, Sayli U, Yavuz O, Uraş I, Dogruel H. Indicators of successful use of the Pavlik harness in infants with developmental dysplasia of the hip. Int Orthop 2007;31:145–50.
[5] Kubo H, Pilge H, Weimann-Stahlschmidt K, Stefanovska K, Westhoff B, Krauspe R. Use of the Tübingen splint for the initial management of severely dysplastic and unstable hips in newborns with DDH: an alternative to Fettweis plaster and Pavlik harness. Arch Orthop Trauma Surg 2018;138:149–53.
[6] Shorter D, Hong T, Osborn DA. Cochrane Review: Screening programmes for developmental dysplasia of the hip in newborn infants. Evidence-based Child Health: A Cochrane Review Journal 2013;8:11–54.
[7] Mehdizadeh M, Dehnavi M, Tahmasebi A, Mahlisha Kazemi Shishvan SA, Babakhan Kondori N, Shahnazari R. Transgluteal ultrasonography in spica cast in postreduction assessment of developmental dysplasia of the hip. J Ultrasound 2020;23:509–14.
[8] Graf R. Fundamentals of sonographic diagnosis of infant hip dysplasia. J Pediatr Orthop 1984;4:735–40.
[9] Shorter D, Hong T, Osborn DA. Screening programmes for developmental dysplasia of the hip in newborn infants. Cochrane Database Syst Rev 2011.
[10] Hareendranathan AR, Chahal BS, Zonoobi D, Sukhdeep D, Jaremko JL. Artificial intelligence to automatically assess scan quality in hip ultrasound. Indian Journal of Orthopaedics 2021;55:1535–42.
[11] Liu B, Hu X, Li L, Gao S. Morphological development of the hip in normal infants under six months of age by the Graf ultrasound method. Front Pediatr 2022;10:914545.
[12] Momani S, Abu Arqub O, Maayah B. Piecewise optimal fractional reproducing kernel solution and convergence analysis for the Atangana–Baleanu–Caputo model of the Lienard's equation. Fractals 2020;28:2040007.
[13] Abu Arqub O, Shawagfeh N. Solving optimal control problems of Fredholm constraint optimality via the reproducing kernel Hilbert space method with error estimates and convergence analysis. Mathematical Methods in the Applied Sciences 2021;44:7915–32.
[14] Abo-Hammour Z, Abu Arqub O, Momani S, Shawagfeh N. Optimization solution of Troesch's and Bratu's problems of ordinary type using novel continuous genetic algorithm. Discret Dyn Nat Soc 2014;2014:401696.
[15] Arqub OA, Abo-Hammour Z. Numerical solution of systems of second-order boundary value problems using continuous genetic algorithm. Inf Sci 2014;279:396–415.
[16] Nobel SN, Sifat OF, Islam MR, Sayeed MS, Amiruzzaman M. Enhancing GI Cancer Radiation Therapy: Advanced Organ Segmentation with ResECA-U-Net Model. Emerging Science Journal 2024;8:999–1015.
[17] Kurdthongmee W, Kurdthongmee P. Fast and Accurate Pupil Estimation Through Semantic Segmentation Fine-Tuning on a Shallow Convolutional Backbone. HighTech and Innovation Journal 2024;5:447–61.
[18] Lebedev IS, Sukhoparov ME. Improving the Quality Indicators of Multilevel Data Sampling Processing Models Based on Unsupervised Clustering. Emerging Science Journal 2024;8:355–71.
[19] Hareendranathan AR, Zonoobi D, Mabee M, Cobzas D, Punithakumar K, Noga M, et al. Toward automatic diagnosis of hip dysplasia from 2D ultrasound. In: 2017 IEEE 14th International Symposium on Biomedical Imaging (ISBI 2017): IEEE; 2017. p. 982–5.
[20] Sezer A, Sezer HB. Deep convolutional neural network-based automatic classification of neonatal hip ultrasound images: A novel data augmentation approach with speckle noise reduction. ultrasound in medicine & biology. 2020;46:735-49.
[21] Atalar H, Üreten K, Tokdemir G, Tolunay T, Çiçeklidağ M, Atik OŞ. The Diagnosis of Developmental Dysplasia of the Hip From Hip Ultrasonography Images With Deep Learning Methods. J Pediatr Orthop 2023;43:e132–7.
[22] Lee S-W, Ye H-U, Lee K-J, Jang W-Y, Lee J-H, Hwang S-M, et al. Accuracy of new deep learning model-based segmentation and key-point multi-detection method for

ultrasonographic developmental dysplasia of the hip (DDH) screening. Diagnostics 2021;11:1174.

[23] Xu J, Xie H, Liu C, Yang F, Zhang S, Chen X, et al. Hip landmark detection with dependency mining in ultrasound image. IEEE Trans Med Imaging 2021;40: 3762–74.

[24] Park HS, Jeon K, Cho YJ, Kim SW, Lee SB, Choi G, et al. Diagnostic performance of a new convolutional neural network algorithm for detecting developmental dysplasia of the hip on anteroposterior radiographs. Korean J Radiol 2021;22:612.

[25] El-Hariri H. Reliable and robust hip dysplasia measurement with three-dimensional ultrasound and convolutional neural networks. University of British Columbia; 2020.

[26] Bilynsky Y, Nikolskyy A, Revenok V, Pogorilyi V, Smailova S, Voloshina O, et al. Convolutional neural networks for early computer diagnosis of child dysplasia. Informatyka, Automatyka, Pomiary w Gospodarce i Ochronie Środowiska 2023;13: 56–63.

[27] Jaremko JL, Hareendranathan A, Bolouri SES, Frey RF, Dulai S, Bailey AL. AI aided workflow for hip dysplasia screening using ultrasound in primary care clinics. Sci Rep 2023;13:9224.

[28] Hu X, Wang L, Yang X, Zhou X, Xue W, Cao Y, et al. Joint landmark and structure learning for automatic evaluation of developmental dysplasia of the hip. IEEE J Biomed Health Inform 2021;26:345–58.

[29] Ojala T, Pietikainen M, Maenpaa T. Multiresolution gray-scale and rotation invariant texture classification with local binary patterns. IEEE Trans Pattern Anal Mach Intell 2002;24:971–87.

[30] Calvillo AD, Vazquez RA, Ambrosio J, Waltier A. Face recognition using histogram oriented gradients. International Symposium on Intelligent Computing Systems: Springer; 2016. p. 125–33.

[31] Goldberger J, Hinton GE, Roweis S, Salakhutdinov RR. Neighbourhood components analysis. Adv Neural Inf Proces Syst 2004;17:513–20.

[32] Liu H, Setiono R. Chi2: Feature selection and discretization of numeric attributes. In: Proceedings of 7th IEEE International Conference on Tools with Artificial Intelligence: IEEE; 1995. p. 388–91.

[33] Kononenko I. Estimating attributes: Analysis and extensions of RELIEF. European conference on machine learning: Springer; 1994. p. 171–82.

[34] Maillo J, Ramírez S, Triguero I, Herrera F. kNN-IS: An Iterative Spark-based design of the k-Nearest Neighbors classifier for big data. Knowl-Based Syst 2017;117: 3–15.

[35] Vapnik V. The support vector method of function estimation. Nonlinear Modeling: Springer; 1998. p. 55–85.

[36] Poyraz E, Cruz RL. Distributed opinion estimation using iterative majority voting. In: 2011 45th Annual Conference on Information Sciences and Systems: IEEE; 2011. p. 1–6.

[37] Shafique K, Shah M. A noniterative greedy algorithm for multiframe point correspondence. IEEE Trans Pattern Anal Mach Intell 2005;27:51–65.

[38] Dogan A, Akay M, Barua PD, Baygin M, Dogan S, Tuncer T, et al. PrimePatNet87: Prime pattern and tunable q-factor wavelet transform techniques for automated accurate EEG emotion recognition. Comput Biol Med 2021;138:104867.

[39] Simonyan K, Zisserman A. Very deep convolutional networks for large-scale image recognition. arXiv preprint arXiv:14091556. 2014.

[40] He K, Zhang X, Ren S, Sun J. Deep residual learning for image recognition. Proceedings of the IEEE conference on computer vision and pattern recognition2016. p. 770-8.

[41] Sandler M, Howard A, Zhu M, Zhmoginov A, Chen L-C. Mobilenetv2: Inverted residuals and linear bottlenecks. Proceedings of the IEEE conference on computer vision and pattern recognition2018. p. 4510-20.

[42] Szegedy C, Zaremba W, Sutskever I, Bruna J, Erhan D, Goodfellow I, et al. Intriguing properties of neural networks. arXiv preprint arXiv:13126199. 2013.

[43] Gong B, Shi J, Han X, Zhang H, Huang Y, Hu L, et al. Diagnosis of infantile hip dysplasia with B-mode ultrasound via two-stage meta-learning based deep exclusivity regularized machine. IEEE J Biomed Health Inform 2021;26:334–44.

[44] Yılmaz, T., & Aydogmus, O. Deep deterministic policy gradient reinforcement learning for collision-free navigation of mobile robots in unknown environments. *Firat University Journal of Experimental and Computational Engineering*, *2*(2), 87-96. 2023.

[45] Sevinç A, Özyurt F. Classification of recyclable waste using deep learning architectures. Firat University Journal of Experimental and Computational Engineering 2022;1(3):122–8.

[46] Demir K, Yaman O. A HOG Feature Extractor and KNN-Based Method for Underwater Image Classification. Firat University Journal of Experimental and Computational Engineering 2024;3(1):1–10.

[47] Soylu E, Gül S, Aslan K, Türkoğlu M, Terzi M. Vision Transformer Based Classification of Neurological Disorders from Human Speech. Firat University Journal of Experimental and Computational Engineering 2024;3(2):160–74.

Sefa Key completed his orthopedics specialization in 2019 and has been working as an Associate Professor in the Department of Orthopedics at Fırat University since 2023. He is interested in orthopedic oncology, sports surgery and trauma surgery. He has multiple publications on artificial intelligence and oncology and continues his research on these topics.

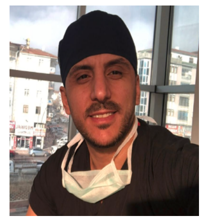

Huseyin Kurum received his specialization training in orthopedics and traumatology from Firat University, Elazig, Turkey, in 2016 and 2021. Between 2021 and 2024, he worked as a specialist physician at Ergani State Hospital in the field of sports medicine arthroscopy and arthroplasty. Starting from the second half of 2024, he has working in Elazığ, Fethi Sekin Training and Research Hospital.He conducts studies in the fields of sports medicine, arthroscopy, ankle surgery, arthroplasty and trauma.

Omer Esmez graduated from Fırat University Faculty of Medicine in 2017 and works as a specialist doctor at Fırat University Orthopedics and Traumatology Department. He has worked in the fields of sports surgery, arthroplasty and trauma surgery. He conducts multiple scientific research on artificial intelligence and gait analysis.

Abdul Hafeez Baig is a professor in information systems at UniSQ. He specializes in information systems, especially how it relates to the healthcare sector as a field of research. He has interest in the re-engineering of business processes

Rena Hajiyeva received my education from 1961 to 1971 at Secondary School No. 132 in Baku. In 1977, I graduated from the Azerbaijan Oil and Industry University with a degree in mechanical engineering. From 1971 to 1990, I worked at the Computing Center of Baku State University as a laboratory assistant, engineer, and senior engineer. From 1990 to 1997, I served as a teacher and head teacher at the Azerbaijan Institute of Applied Sciences. Since 1997, I have been working as an associate professor and professor at the Western Caspian University, at the Department of Mathematics and Computer Technologies. In 2007, I defended my doctoral dissertation on Teaching Methods of Informatics Related to Mathematics and Physics; and received a PhD in pedagogy, and in 2008, I was awarded the title of associate professor. My scientific interests include mathematics, physics, finance, and programming. Since 2011, I have been serving as the head of the Department of Information Technologies at Western Caspian University. I am the author of more than 100 scientific works, including methodological tools, textbooks, and scientific articles..

Sengul Dogan received the master's degree in bioengineering the Ph.D. degree in electrical and electronics engineering from the Firat University, Elazig, Turkey, in 2007 and 2011, respectively. She is currently a Professor with the Digital Forensics Engineering, Technology Faculty, Firat University. Her main research interests include computer forensics, mobile forensics, image processing, and signal processing. She has been working actively on developing algorithms in machine learning for biomedical data

Turker Tuncer received the master's degree in electronics and computer sciences and the Ph.D. degree in software engineering from Firat University, Elazig, Turkey, in 2011 and 2016, respectively. He is currently an Associate Professor with the Digital Forensics Engineering, Technology Faculty, Firat University. His main research interests include feature engineering, image processing, signal processing, information security, and pattern recognition. He has been working actively on developing algorithms in machine learning applied to visual surveillance and biomedical data.